The quasi-band-structure description of conjugated oligomers

2000 J. Phys.: Condens. Matter 12 1753

(http://iopscience.iop.org/0953-8984/12/8/317)

J. Phys.: Condens. Matter **12** (2000) 1753–1768. Printed in the UK PII: S0953-8984(00)08568-4

The quasi-band-structure description of conjugated oligomers

E Zojer†, M Knupfer‡, Z Shuai§, J L Brédas§‖, J Fink‡ and G Leising†

† Institut für Festkörperphysik, Technische Universität Graz, Petersgasse 16, A-8010 Graz, Austria

‡ Institut für Festkörper- und Werkstofforschung Dresden, Postfach 270016, D-01171 Dresden, Germany

§ Service de Chimie des Matériaux Nouveaux, Centre de Recherche en Electronique et Photonique Moléculaires, Université de Mons-Hainaut, Place du Parc 20, B-7000 Mons, Belgium

‖ Department of Chemistry, The University of Arizona, PO Box 210041, Tucson, AZ 85721-0041, USA

E-mail: egbert@ffphal01.tu-graz.ac.at (E Zojer)

Received 16 October 1999, in final form 24 November 1999

Abstract. We have investigated momentum dependent excitations in conjugated organic oligomer materials. Theoretical simulations based on the intermediate neglect of differential overlap (INDO) approach coupled to a single configuration interaction (SCI) technique considering the proper transition matrix elements for inelastic electron scattering are compared to experimental electron energy-loss spectroscopy (EELS) investigations. In this work we concentrate on sexiphenyl (6P), sexithienyl (6T) and beta-carotene. 6P and 6T are widely used in a number of electronic and optoelectronic devices and together with beta-carotene they can be regarded as model substances for the three big classes of conjugated polymer materials, namely phenylenes, thiophenes and acetylenes. Both experimental and theoretical results underline the validity of the so called quasi-band-structure model for the description of periodic molecules with only a finite number of repeat units. We also highlight the influence of chain orientation on EELS spectra and discuss the reasons for certain deviations between molecule-based simulations and the excitation processes occurring in the actual molecular crystals upon inelastic electron scattering.

1. Introduction

Conjugated organic materials are of particular interest due to many interesting applications in a number of electronic and optoelectronic devices ranging from light emitting devices [1] and solar cells [2] to fully organic transistors [3]. Phenylene-based materials, like sexiphenyl (6P) studied here are especially important because of their emission in the blue spectral range [4]; sexithienyl (6T) (also discussed in this paper) has been the first material used in an organic transistor and beta-carotene (the third oligomer, whose quasi-band structure is described here) can be regarded as the model oligomer of poly(acetylene), a material whose conductivity has been changed by 14 orders of magnitude upon doping [5], thus exceeding the values found in common metals. Moreover, most of the currently investigated conjugated organic materials are built of phenylene, thienylene and vinylene (acetylene) repeat units. Therefore, the present study deals with model systems for a wide range of commonly used conjugated polymers and oligomers and the basic results presented here can be regarded to be characteristic of organic molecular crystals consisting of molecules with a certain number of repeat units. The chemical structures of 6P, 6T and beta-carotene are shown in figure 1.

0953-8984/00/081753+16$30.00

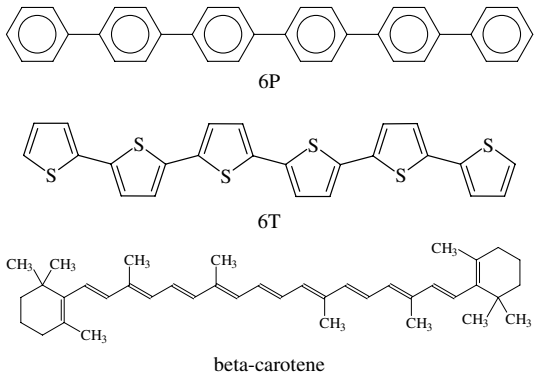

Figure 1. Chemical structures of sexiphenyl (6P), sexithienyl (6T) and beta-carotene.

The study of *conjugated oligomers* as presented here is especially attractive for the following reasons. (i) Finite-size systems can be obtained with high purity and a well defined chemical structure and conjugation length. (ii) The obtained films usually display a high degree of crystallinity, on the one hand helping to obtain strong texturing by aligning the crystallites and, on the other hand allowing a characterization of the molecular orientation in the films by x-ray and elastic electron diffraction. (iii) Additionally, basic electronic properties like the band gap can be extrapolated from oligomers to polymers by simple scaling laws [6]. It has been shown recently for phenylene based materials that, in fact, the full band structure gradually evolves out of molecular levels as the chain length and therefore the number of repeat units increases [7]. (iv) Even in polymer samples usually limited conjugation lengths are found as a result of synthesis conditions. Therefore, these materials are very well described by oligomers with a large number of repeat units.

When performing optical spectroscopy only excitations with essentially zero momentum transfer are induced. However, significantly more information about the actual electronic properties of a certain material and about the description of the electronic states in momentum space can be gained, if in the excitation process both the transferred energy and the transferred momentum can be varied. This is achieved, for instance, by inelastic electron scattering (electron energy-loss spectroscopy (EELS) [8]). An excitation process including a finite momentum transfer $\boldsymbol{q}$ corresponds to a non-vertical transition in a bandlike description in momentum space. Therefore in conjugated polymers with continuous strongly dispersing bands one observes a steady shift of the inter-band transitions as a function of $\boldsymbol{q}$ [8]. For finite size systems the dispersion is not continuous; instead there is a shift of oscillator strength to higher lying discrete excited states as the value of momentum transfer increases [9–11]. This has been explained [9] in the framework of the so called *quasi-band structure* (QBS): in this model the discrete occupied and unoccupied molecular levels are aligned in momentum space along the bands derived for the corresponding infinite system (see figure 2) [7, 9, 10] (compare also the approaches described in [12] and [13]). This means that the electronic properties of the molecular crystal are primarily determined by the molecular building blocks and inter-chain interaction effects can be regarded as a 'second order correction'. However, they have to be considered, when describing optical absorption, for which a much better resolution than in EELS spectra can be achieved. The dependence of the photo-electron emission intensity in 6P on the photon energy also supports the QBS model [14]. For the QBS description of oligomer systems it is important to mention that each molecular eigenstate has to be described

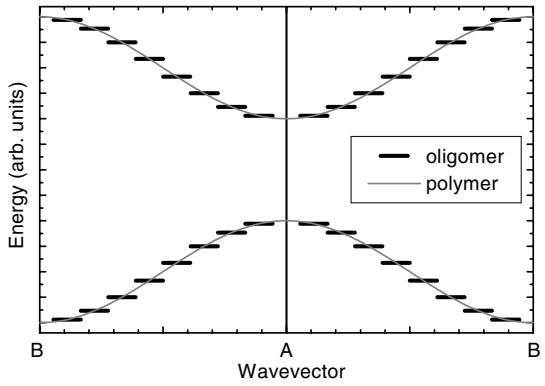

Figure 2. Schematic comparison of the momentum dependent description of the electronic states in conjugated polymers with infinite periodicity and of an arbitrary oligomeric system containing eight repeat units (compare [7, 9, 10]). For poly(*para*-phenylene) (PPP) and the related model oligomer sexiphenyl (6P) as well as for poly(thienyl) and sexithienyl (6T) the point on the momentum axis denoted by A corresponds to the zone centre, whereas B denotes the boundary of the first Brillouin zone (given by π/a). In *trans*-poly(acetylene) and beta-carotene this assignment is reversed. (For a compilation of polymer band-structures see e.g. André J-M and Delhalle J 1991 *Quantum Chemistry Aided Design of Organic Polymers* (Singapore: World Scientific) and references therein.) In finite-size systems the electron momentum (given by $\hbar\boldsymbol{k}$, with $\boldsymbol{k}$ denoting the wavevector) is no longer a good quantum number. Therefore in that case each eigenstate has to be characterized by a certain momentum range, rather than by a single value of $\boldsymbol{k}$ [14].

in momentum space by a $+\boldsymbol{k}$ and a $-\boldsymbol{k}$ component ($\boldsymbol{k}$ corresponding to the electron wavevector), because in a molecular description dealing with finite size systems the total value of $\boldsymbol{k}$ for each eigenstate has to be zero [7, 10, 14].

To be able to assign the various peaks in momentum dependent EELS spectra to certain transitions inside the molecule and to evaluate the importance of correlation effects, we have performed semiempirical intermediate neglect of differential overlap (INDO) [15] calculations coupled to a single configuration interaction (SCI) method implementing the proper momentum dependent transition matrix elements. The SCI approach allows to characterize the importance of correlation effects on the various excited states. The method applied here has been successfully used to theoretically study the evolution of the electronic states with chain length for phenylene based materials [7] and to describe momentum dependent excitation processes in poly(acetylene) and poly(*para*-phenylenevinylene) [16].

2. Theoretical and experimental methodology

The geometry of the 6P molecule is optimized with the semiempirical Hartree–Fock Austin Model 1 (AM1) method, which provides good estimates of geometries and heats of formation for organic molecules in their ground state [17]. The inter-ring twist angles are set to 22.7° [18], instead of the 40° obtained for fully geometry-optimized isolated oligophenylenes [19], to account for packing effects in the solid state. The resulting simulated inelastic scattering spectra are very similar to those obtained when using the 6P geometry derived from x-ray scattering experiments, in spite of the fact that in [20] the molecule is on average planar. This is due to a slight distortion of inter- and intra-ring bonds (resulting from the achieved accuracy in these x-ray investigations—see e.g. the calculations in [21]), which like an inter-ring twist reduces conjugation along the molecular backbone. For 6T and beta-carotene, we have based our

calculations on geometries derived from x-ray diffraction data from [22] and [23], respectively. Calculations performed for AM1 optimized geometries give similar results [24].

The energies and wavefunctions of the ground and various excited states are calculated on the basis of the semiempirical Hartree–Fock intermediate neglect of differential overlap (INDO) method, parametrized by Zerner and co-workers [25] with the Coulomb repulsion terms expressed via the Mataga–Nishimoto potential [26]. For the description of excited states a linear combination of Slater determinants generated by promoting an electron from an occupied to an unoccupied level is used. This single configuration-interaction technique (SCI) allows us, in contrast to e.g. standard band structure techniques, to include electron correlation effects in the calculations. As a consequence one encounters a coupling between various single particle transitions as a function of the energy and momentum transferred in the excitation process.

The differential cross-section characterizing the inelastic scattering process of an electron in the framework of the first Born approximation is given by [27]

$$\frac{\partial^2\sigma}{\partial\Omega\partial(\hbar\omega)} \propto \frac{1}{|\boldsymbol{q}|^4}\sum_f \left|\left\langle \Psi_f \left| \sum_{n=1}^{N} \mathrm{e}^{-\mathrm{i}\boldsymbol{q}\cdot\boldsymbol{r}_n} \right| \Psi_i \right\rangle\right|^2 \delta(E_f - E_i - \hbar\omega) \tag{1}$$

with i denoting the initial state (with energy E_i) and f the final state (with energy E_f) of the sample. $\hbar\omega$ is the energy and $\hbar\boldsymbol{q}$ the momentum transferred during the interaction. The summation (index n) extends over the electrons of the probed system. The matrix elements in equation (1) are calculated from the INDO/SCI wavefunctions for transitions between the ground and various excited states as a function of $\boldsymbol{q}$ in the zero differential overlap (ZDO) approximation. The spectra shown in the following sections have been obtained by a convolution of the calculated transition energies with Gaussian functions, weighted by the momentum dependent transition matrix elements. For the following discussion it is important to point out that the transition matrix element is *not linear* with respect to the transferred momentum $\boldsymbol{q}$. This is in sharp contrast to an optical dipole transition, for which the matrix element is simply proportional to the electric field of the incoming photons.

The simulated spectra are compared to transmission EELS data. These have been obtained using a spectrometer with a primary energy of 170 keV, the details of the experimental set-up being described elsewhere [8]. The energy and momentum resolution for the selected beam settings are 0.12 eV and 0.05 Å^{-1}, respectively. During all measurements the samples are kept at room temperature. We note that, while the measurements are carried out on crystalline oligomer films, the calculations are performed for single molecules only. Thus, solid state screening effects are not considered. They can lead to small changes in the spectral shape and energetic position of the excitations.

Highly oriented films of 6P have been obtained by evaporating a thin layer of 6P (about 50 Å) onto a NaCl substrate, unidirectionally rubbing that layer in the NaCl[100] direction and subsequently depositing another 1000 Å of 6P on the substrate [28]. This procedure using a deposition rate of about 2 Å min^{-1} and keeping the crystal at ambient temperature yields highly textured films with 6P chains lying parallel to the surface of the substrate in the direction of the rubbing process, as shown by elastic electron diffraction [24]. For 6T we have obtained a quasi-epitaxial growth of the molecules on an untreated NaCl crystal, with chains at every 45° corresponding to a growth along the crystal's ⟨100⟩ and ⟨110⟩ directions. To obtain freestanding samples, which are essential for transmission electron spectroscopy, the films are floated off the NaCl crystals in distilled water and subsequently fixed to Cu electron-microscopy grids.

3. Results and discussion

3.1. Sexiphenyl

In figure 3 the simulated differential cross-sections for sexiphenyl (6P) molecules are shown for momentum transfer $\boldsymbol{q}$ parallel to the molecular axes as well as for angles of 30, 60 and 90° between $\boldsymbol{q}$ and the chain direction. In the low energy range there are five distinct maxima at 3.72 eV, 4.23 eV, 4.71 eV, 5.15 eV and 5.55 eV, respectively (peaks I to V). Upon increasing the value of momentum transfer oscillator strength is shifted from the low energy transitions to the higher lying excited states. This behavior can be well understood within the framework of the quasi-band structure [7, 9, 10] outlined in the introduction and sketched in figure 4. For the case of 6P, six occupied and six unoccupied states are aligned along the dispersing bands of the corresponding polymer in momentum space. These delocalized orbitals are characterized by high electron densities at the carbon atoms forming the inter-ring bridges which leads to a strong interaction between the corresponding benzene states and therefore to a strong splitting of the orbital energies. In oligophenylenes and related organic materials in addition to the delocalized states there are orbitals with vanishing electron densities at the carbon atoms of the inter-ring bridges. These orbitals have similar eigenenergies and are denoted as localized states.

For zero momentum transfer the excitation process in momentum space can be described as a vertical transition which mainly involves the HOMO and the LUMO states (to a certain extent also the HOMO − 1 and HOMO + 1 as well as the HOMO − 2 and LUMO + 2 levels as evident in table 1). Upon increasing the value of momentum transfer the transitions become more and more 'diagonal' in nature resulting in a shift of oscillator strength to an excited state at 4.23 eV, which according to table 1 is described by coupled HOMO − 1 to LUMO and HOMO to LUMO + 1 transitions. The excited state at 4.71 eV is dominated by Slater determinants characterized by the HOMO to LUMO + 2, the HOMO − 1 to LUMO + 1 and the HOMO − 2 to LUMO transitions (see table 1). Considering the 6P QBS as depicted in figure 4 it can be well understood that the latter peak reaches its maximum for even higher values of momentum transfer. The strong coupling between certain groups of single particle transitions can be explained by the similar energies and values of momentum transfer associated with the corresponding promotions of an electron from an occupied to an unoccupied level, as evidenced by the arrows in figure 4.

Table 1. Energies and CI expansion coefficients of the dominant excited states in 6P (H and L denote the HOMO and LUMO levels.) All excitations contained in this table are polarized parallel to the long molecular axis of 6P.

Peak	Energy (eV)	CI expansion coefficients
I	3.72	$-0.88[\mathrm{H} \rightarrow \mathrm{L}] - 0.38[\mathrm{H} - 1 \rightarrow \mathrm{L} + 1] - 0.18[\mathrm{H} - 2 \rightarrow \mathrm{L} + 2]$
II	4.23	$0.69[\mathrm{H} \rightarrow \mathrm{L} + 1] + 0.61[\mathrm{H} - 1 \rightarrow \mathrm{L}] + 0.21[\mathrm{H} - 1 \rightarrow \mathrm{L} + 2] + 0.17[\mathrm{H} - 2 \rightarrow \mathrm{L} + 1]$
III	4.71	$-0.64[\mathrm{H} \rightarrow \mathrm{L} + 2] - 0.54[\mathrm{H} - 1 \rightarrow \mathrm{L} + 1] - 0.41[\mathrm{H} - 2 \rightarrow \mathrm{L}]$
IV	5.15	$-0.61[\mathrm{H} \rightarrow \mathrm{L} + 9] - 0.50[\mathrm{H} - 1 \rightarrow \mathrm{L} + 2] - 0.42[\mathrm{H} - 2 \rightarrow \mathrm{L} + 1] + 0.23[\mathrm{H} - 9 \rightarrow \mathrm{L}]$
V	5.55	$0.52[\mathrm{H} \rightarrow \mathrm{L} + 10] + 0.44[\mathrm{H} - 1 \rightarrow \mathrm{L} + 9] + 0.35[\mathrm{H} - 2 \rightarrow \mathrm{L} + 2] - 0.28[\mathrm{H} - 5 \rightarrow \mathrm{L}]$ $-0.24[\mathrm{H} \rightarrow \mathrm{L} + 3]$

All excited states listed in table 1 are polarized parallel to the molecular axis as can be seen in figure 3. In the higher energy range there is another parallel polarized peak (VII) in the energy range between 6.2 eV and 6.4 eV, which in fact is a superposition of transitions to various excited states with similar energies but momentum dependent oscillator

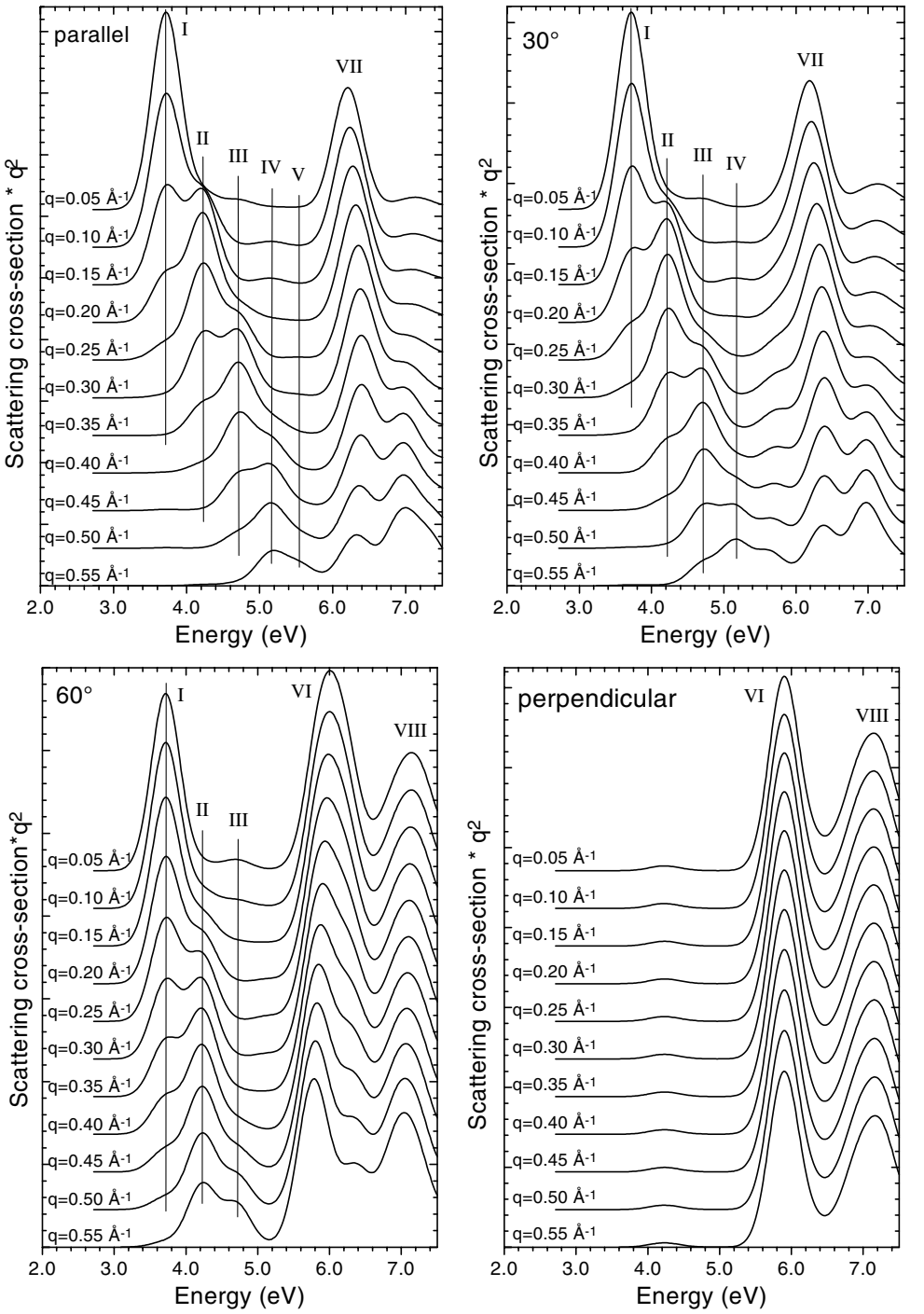

Figure 3. INDO/SCI simulated differential scattering cross-section in 6P as a function of the angle between the direction of momentum transfer $\boldsymbol{q}$ and the chain axis. The cross-sections are multiplied by q^2, because this roughly corresponds to the normalization usually applied when plotting the experimental data. For all spectra $\boldsymbol{q}$ is in the plane of half of the benzene rings. (The inter-ring twist angle is set to 22.7°.)

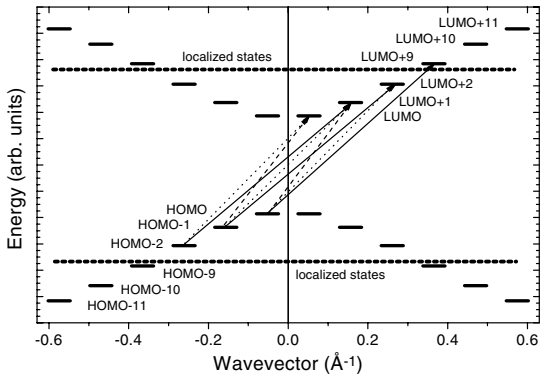

Figure 4. Schematic representation of the 6P molecular states in a quasi-band description. The delocalized orbitals are reminiscent of dispersing bands, whereas the localized states are characterized by similar energies. The value for a (the size of the repeat unit) is taken from the AM1 optimizations. The arrows denote the single particle transitions with the most significant contributions to peak II (dashed), peak III (dotted) and peak IV (solid) from table 1 and figure 3.

strengths. The CI description of these states is dominated by single particle transitions between localized orbitals. Peak VI (between 5.8 eV and 6.0 eV) and peak VIII (between 7.0 eV and 7.2 eV) are polarized perpendicular to the molecular axis in agreement with optical simulations for oligo(phenylene)s [24] and oligo(phenylenevinylene)s [29]. They also consist of transitions to a number of different excited states, which in the CI expansion are, however, dominated by single particle transitions from localized to delocalized orbitals and vice versa.

Upon increasing the angle Θ between the molecular axis and the direction of momentum transfer several effects are observed: (i) The intensities of the 'parallel' transitions are strongly reduced (proportional to $\cos^2(\Theta)$). (ii) For momentum transfer perpendicular to the chain peak VI and peak VIII dominate the spectrum. (iii) In addition to (i) and (ii), which are also observed in optical investigations, in inelastic electron-scattering processes the momentum dependence of the observed spectra is strongly affected by the angle between the molecular axis and the direction of momentum transfer. Consequently, the shift of oscillator strength to higher energy excitations with increasing $\boldsymbol{q}$ is reduced with chain misalignment. For example, the shape of the spectra in the low energy region up to about 5 eV for momentum transfer parallel to the chains corresponds to that calculated for twice the value of q at a twist angle of 60°. This indicates that in the low energy region inelastic scattering processes in highly anisotropic media, like conjugated polymers and oligomers, can be well described by the component of momentum transfer projected on the axis along which the electron wavefunctions are delocalized (compare [9]). To quantitatively derive the dispersion and width of the bands of anisotropic materials from the $\boldsymbol{q}$ dependent shifts of peak positions and oscillator strengths it is therefore essential to perform investigations on highly textured samples.

The experimental EELS spectrum of a highly textured 6P film for momentum transfer parallel to the molecular axis is shown in figure 5. There is good agreement between the measured loss function and the calculated scattering cross-section in figure 3 concerning the number of the peaks as well as their intensity variation.

There are, however, also deviations between the experimental spectra and the simulations, which will be discussed in the following:

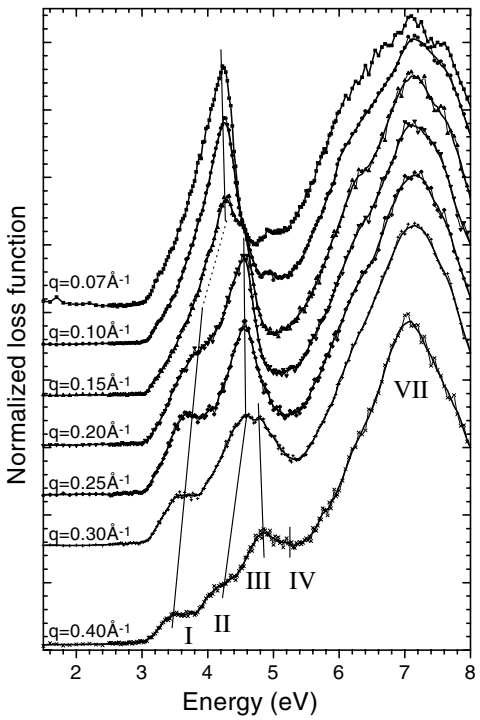

Figure 5. Normalized loss function of a highly textured 6P thin film for momentum transfer parallel to the molecular axis.

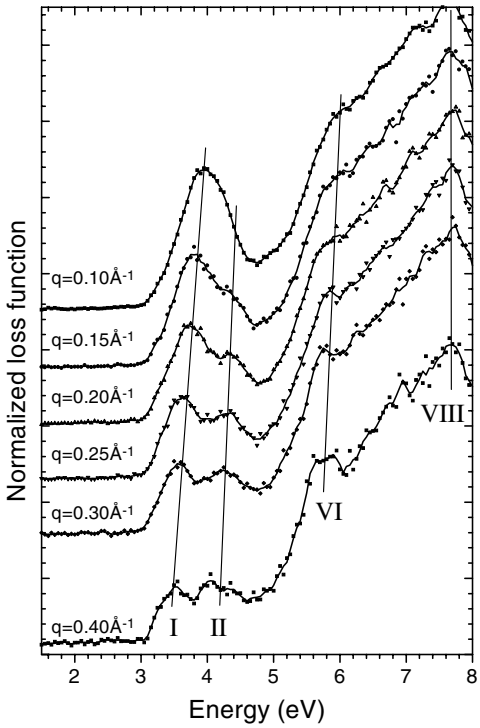

Figure 6. Normalized loss function of a highly textured 6P thin film for momentum transfer perpendicular to the molecular axis.

(i) Compared to the simulations, the experimental spectra are slightly shifted to higher energies. This can be explained by inter-chain interaction effects as shown in [24] and [30]. Additionally, the 6P energy gap strongly depends on the twist angle between the benzene rings and a slight increase of the inter-ring twist also shifts the spectra to higher energies [24]. Moreover, screening effects as described in the methodology section and in the following paragraph also influence the actual positions of the maxima observed in an electron energy-loss experiment.

(ii) In the experiment, the peaks I to IV shift to lower energies with increasing q, especially when higher lying maxima gain oscillator strength. This is a consequence of the fact that in EELS one excites density oscillations of the electron system. Therefore, when describing energy-loss experiments by means of the dielectric function (with the real part denoted by ε_1 and the imaginary part by ε_2) the cross-section is found to be proportional to [8]

$$\frac{\partial^2\sigma}{\partial\Omega\partial(\hbar\omega)} \propto \mathrm{Im}\left(\frac{1}{\varepsilon}\right) = \frac{\varepsilon_2}{\varepsilon_1^2+\varepsilon_2^2}. \tag{2}$$

We have performed calculations using a Lorentz model to describe dielectric functions with varying oscillator strengths of transitions at slightly different energies (as found e.g. in 6P). The results indicate a shift of a maximum in the loss function to lower energies, if a further transition at slightly higher energy gains intensity, provided that ε_1 in this energy range falls below zero. In this case the position of the peak in the loss function is primarily

determined by the zero-crossing of ε_1 rather than by a maximum of ε_2. This reflects the fact that both the real and the imaginary part of the dielectric function contribute to the density response; i.e. dynamic screening of the excitations, as described by ε_1, to a certain extent influences the observed spectra. As our calculations only consider isolated molecules we do not take into account the screening contributions completely. This interpretation of the peak shift is supported by the fact that, e.g. peak I remains at virtually the same energy for $q = 0.07$ Å^{-1}, $q = 0.1$ Å^{-1} and $q = 0.15$ Å^{-1}. The negative dispersion starts for higher values of q, when peak II and peak III become dominant. Peak II also starts to shift only for $q = 0.4$ Å^{-1} when peak III is the dominant spectral feature in the low energy region. In addition to the screening effect described above the actual three dimensional band structure of the 6P molecular crystal also results in deviations from the molecular simulations. Density-functional-theory-based band-structure calculations for poly(*para*-phenylenevinylene) [31], as well as for oligophenylenes [21] and poly(*para*-phenylene) [32], yield very complex bands for a momentum vector perpendicular to the chain axes. In the phenylene-based materials [21, 32] even an indirect energy gap is found. These properties can also be held responsible for the shift of the peaks in the EELS spectra.

(iii) The relatively high intensity of the broad maximum around 7 eV and the weak shoulders at 5.9 eV and 7.6 eV in the experimental spectra of figure 5 are partly due to contributions of misaligned chains.

The latter features correspond to the transitions polarized perpendicular to the molecular axis and are strongly enhanced in the spectra recorded with momentum transfer perpendicular to the chain direction as depicted in figure 6. The double peak structure between 3 eV and 4.5 eV with an increasing intensity of the second peak for higher values of $\boldsymbol{q}$ in figure 6 is reminiscent of the calculations for large angles between the molecular axis and the direction of momentum transfer in figure 3. Therefore, one can attribute the low energy features up to an energy of 4.5 eV in the spectra in figure 6 to contributions of misaligned molecules, for which the angle between the chain direction and the $\boldsymbol{q}$ vector is less than 90°.

3.2. Sexithienyl (6T)

In the experimentally investigated 6T film the crystallites grow with the 6T chains aligned along the ⟨100⟩ and ⟨110⟩ axes of the NaCl substrates. The chains are predominantly aligned parallel to the surface of the substrate. The texturing, however, is not as well pronounced as in the 6P film for which the spectra shown in figures 5 and 6 have been obtained. To account for the alignment of the molecules we have simulated the momentum dependent scattering cross-section of 6T by taking a superposition of spectra for momentum transfer parallel and perpendicular to the molecular axis, as well as for an angle of 45° between the chain direction and the $\boldsymbol{q}$ vector, considering both a misorientation in the plane of the thienyl rings as well as perpendicular to it. The results of the simulations are shown in figure 7. They imply that also in 6T, like in 6P, a quasi-band structure evolves, which is characterized by discrete electronic states in momentum space aligned along the bands of the parent polymer. The calculations for 6T have been extended up to a momentum transfer of $q = 0.8$ Å^{-1}, as we have been able to obtain spectra up to that $\boldsymbol{q}$ value (see figure 8). In the simulations the peaks III and IV are slightly asymmetric with a weak additional maximum between them. The origin of this will be discussed below, when analysing the CI expansion coefficients. The theoretically derived quasi-band structure description of the electronic states also for 6T is fully supported by the experimental loss functions shown in figure 8. At about 6 eV also the perpendicularly polarized maximum is visible as a small peak, as predicted by the simulations for the above described texturing of the investigated film.

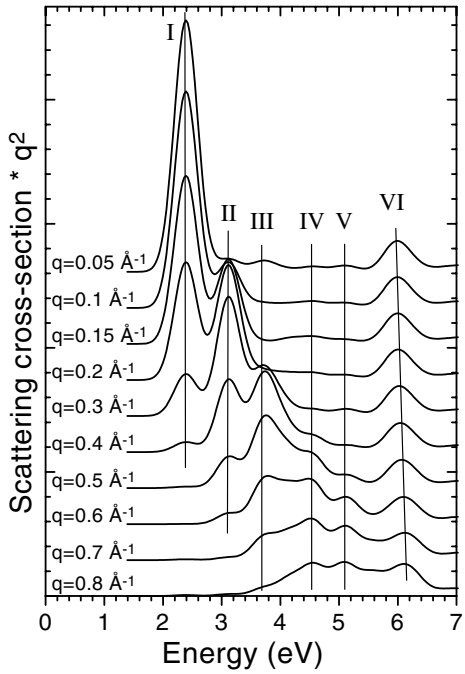

Figure 7. INDO/SCI simulated differential scattering cross-section in 6T. To properly represent the texturing of the experimentally investigated film a superposition of spectra for momentum transfer parallel, at an angle of 45° and perpendicular to the molecular axis is shown. The cross-sections are multiplied by q^2, because this corresponds to the normalization usually applied when plotting the experimental data.

A detailed analysis of the electronic nature of the various excited states gaining significant oscillator strength for certain q values in the investigated energy range is given in table 2. The CI expansions together with the alignment of the molecular levels along the bands of the parent polymers according to the quasi-band description fully explain why the energetically higher lying excited states gain oscillator strength only for increasing values of momentum transfer. So for example for a quasi-band alignment of the molecular levels the HOMO $-$ 3 $\rightarrow$ LUMO and HOMO $-$ 2 $\rightarrow$ LUMO + 1 transitions dominating the description of peak IVb in momentum space are 'more diagonal' than the HOMO $\rightarrow$ LUMO + 2 and HOMO $-$ 1 $\rightarrow$ LUMO + 1 transitions of IIIa, which are again 'more diagonal' than the HOMO $\rightarrow$ LUMO + 1 and HOMO $-$ 1 $\rightarrow$ LUMO transitions characterizing excited state II. The lowest lying state I is dominated by the HOMO $\rightarrow$ LUMO transition. Therefore it is most prominent for vertical (quasi-optical) excitations and excitations with low momentum transfer. The perpendicularly polarized excitations VIa, VIb and VIc all contain strong contributions from transitions from deep lying occupied states or to high lying unoccupied levels.

An interesting effect in 6T is that in contrast to the situation encountered e.g. in 6P the peaks III and IV are split. This means that e.g. for IIIa HOMO $-$ 2 $\rightarrow$ LUMO is very strong and the contribution of HOMO $\rightarrow$ LUMO + 2 is only relatively weak, whereas IIIb is dominated by HOMO $\rightarrow$ LUMO + 2 and contains only a small contribution from HOMO $-$ 2 $\rightarrow$ LUMO. An equivalent CI description is found for IVa and IVb. The splitting of the transitions can be attributed to a *breaking of charge conjugation symmetry* caused by the heteroatoms (sulphur) in the 6T chain.

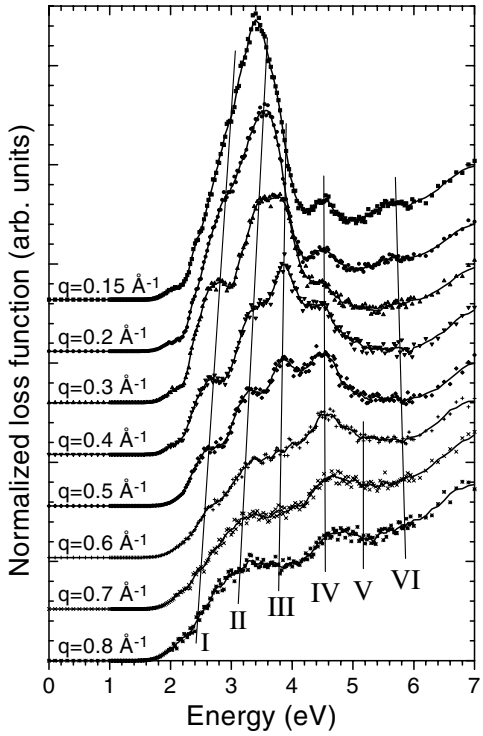

Figure 8. Momentum dependent loss function of a 6T film with molecular axes in the plane of momentum transfer. Due to the quasi-epitaxial growth of the film, in part of the crystallites the molecular axes are parallel to the $\boldsymbol{q}$ direction. As a result of the texturing there are also 6T chains at ± 45, ± 90 and $\pm 135^{\circ}$.

Table 2. Energies and CI expansion of the most significant excited states in a 6T molecule with a geometry derived from [22]. (H refers to the molecular HOMO and L to the LUMO.) Peaks I to V are polarized parallel and peak VI perpendicular to the long molecular axis of 6T.

Peak	Energy (eV)	CI expansion coefficients
I	2.39	$-0.92\,[\mathrm{H} \rightarrow \mathrm{L}] - 0.32[\mathrm{H}-1 \rightarrow \mathrm{L}+1]$
II	3.11	$-0.76\,[\mathrm{H} \rightarrow \mathrm{L}+1] - 0.57[\mathrm{H}-1 \rightarrow \mathrm{L}] + 0.23[\mathrm{H}-1 \rightarrow \mathrm{L}+2]$
IIIa	3.70	$-0.79\,[\mathrm{H} \rightarrow \mathrm{L}+2] + 0.47[\mathrm{H}-1 \rightarrow \mathrm{L}+1] - 0.23[\mathrm{H}-1 \rightarrow \mathrm{L}+3] - 0.18[\mathrm{H}-2 \rightarrow \mathrm{L}]$
IIIb	3.98	$0.76\,[\mathrm{H}-2 \rightarrow \mathrm{L}] - 0.36[\mathrm{H}-1 \rightarrow \mathrm{L}+1] - 0.29[\mathrm{H} \rightarrow \mathrm{L}+2] + 0.24[\mathrm{H}-3 \rightarrow \mathrm{L}+1]$ $-0.21[\mathrm{H}-1 \rightarrow \mathrm{L}+3]$
IVa	4.17	$-0.77\,[\mathrm{H} \rightarrow \mathrm{L}+3] - 0.44[\mathrm{H}-1 \rightarrow \mathrm{L}+2] + 0.25[\mathrm{H}-1 \rightarrow \mathrm{L}+4] - 0.16[\mathrm{H}-2 \rightarrow \mathrm{L}+1]$
IVb	4.56	$0.60\,[\mathrm{H}-3 \rightarrow \mathrm{L}] + 0.55[\mathrm{H}-2 \rightarrow \mathrm{L}+1] + 0.34[\mathrm{H}-1 \rightarrow \mathrm{L}+2]$
V	5.12	$-0.51\,[\mathrm{H}-3 \rightarrow \mathrm{L}+1] + 0.49[\mathrm{H}-4 \rightarrow \mathrm{L}] + 0.45[\mathrm{H}-2 \rightarrow \mathrm{L}+2] - 0.32[\mathrm{H}-1 \rightarrow \mathrm{L}+3]$
VIa	5.92	$-0.44\,[\mathrm{H}-10 \rightarrow \mathrm{L}] - 0.38[\mathrm{H} \rightarrow \mathrm{L}+6] + 0.31[\mathrm{H} \rightarrow \mathrm{L}+13] - 0.29[\mathrm{H}-4 \rightarrow \mathrm{L}]$ $+0.25[\mathrm{H}-1 \rightarrow \mathrm{L}+5]$
VIb	6.00	$-0.44\,[\mathrm{H}-2 \rightarrow \mathrm{L}+2] - 0.38[\mathrm{H}-2 \rightarrow \mathrm{L}+4] + 0.26[\mathrm{H}-4 \rightarrow \mathrm{L}] - 0.23[\mathrm{H}-10 \rightarrow \mathrm{L}]$ $+0.22[\mathrm{H}-1 \rightarrow \mathrm{L}+5]$
VIc	6.12	$-0.44\,[\mathrm{H} \rightarrow \mathrm{L}+13] - 0.31[\mathrm{H} \rightarrow \mathrm{L}+15] + 0.28[\mathrm{H}-10 \rightarrow \mathrm{L}] - 0.27[\mathrm{H}-8 \rightarrow \mathrm{L}]$ $+0.25[\mathrm{H}-3 \rightarrow \mathrm{L}+3]$

3.3. Beta-carotene

For beta-carotene the inelastic scattering cross-section has been calculated for molecules whose C atom positions have been derived from x-ray diffraction data [23]. (The positions of the H

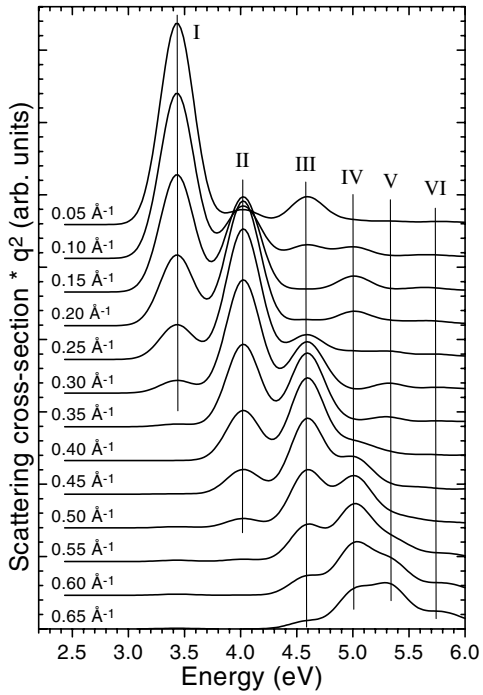

Figure 9. INDO/SCI simulated partial differential scattering cross-section of beta-carotene for an angle of 32.7° between the direction of momentum transfer and the molecular axes. The cross-sections are multiplied by q^2, because this roughly corresponds to the normalization usually applied when plotting the experimental data.

atoms have been refined by AM1 calculations.) As experimental EELS data for beta-carotene single crystals, which do inherently have the highest possible degree of texturing, are available from the literature, we have not performed new experiments for that material but rather compare our theoretical results to the spectra from [9], which in fact were the first example showing the applicability of the QBS description to oligomers. The angle between the *b* axis and the two non-parallel beta-carotene chains of the unit cell is 32.7°. In the experiments the $\boldsymbol{q}$ vector is set parallel to the *b* axis of the beta-carotene single crystal. Following the results of section 3.1, which stress the importance of chain-misalignment effects for the shape of the momentum dependent scattering cross-section in 6P, the spectra shown in figure 9 have been obtained for an angle of 32.7° between the vector of momentum transfer and the beta-carotene chains. Like in 6P and 6T an increase of momentum transfer results in a shift of oscillator strength to higher lying maxima in good agreement with the experimental data in [9]. The calculated energies of the lower lying transitions also agree very well with the experimentally obtained values. The relatively broad peak for $q = 0.65$ Å^{-1}, however, is slightly shifted to higher energies in the experimental investigations. Here the agreement with calculations performed for an AM1 optimized geometry of beta-carotene is better than for the structure derived from x-ray data [24].

An investigation of the CI expansion coefficients of the various excited states (table 3) for beta-carotene also reveals that the shift of oscillator strength to energetically higher lying excited states can be very well explained by the more 'diagonal' character of the corresponding single-particle transitions, provided that the molecular states in momentum space are aligned along dispersing bands.

Table 3. Energies and CI expansion of the most significant excited states in a beta-carotene molecule with a geometry derived from [23]. (H refers to the molecular HOMO and L to the LUMO.) All excitations contained in this table are polarized parallel to the long molecular axis of beta-carotene.

Peak	Energy (eV)	CI expansion coefficients
I	3.43	$0.90\,[\mathrm{H} \rightarrow \mathrm{L}] - 0.36\,[\mathrm{H}-1 \rightarrow \mathrm{L}+1]$
II	4.02	$-0.74\,[\mathrm{H} \rightarrow \mathrm{L}+1] + 0.59\,[\mathrm{H}-1 \rightarrow \mathrm{L}] - 0.20\,[\mathrm{H}-1 \rightarrow \mathrm{L}+2]$
III	4.59	$-0.68\,[\mathrm{H} \rightarrow \mathrm{L}+2] - 0.52\,[\mathrm{H}-1 \rightarrow \mathrm{L}+1] + 0.36\,[\mathrm{H}-2 \rightarrow \mathrm{L}] + 0.20\,[\mathrm{H}-1 \rightarrow \mathrm{L}+3]$
IV	5.01	$-0.62\,[\mathrm{H} \rightarrow \mathrm{L}+3] + 0.52\,[\mathrm{H}-1 \rightarrow \mathrm{L}+2] + 0.34\,[\mathrm{H}-1 \rightarrow \mathrm{L}+1] + 0.21\,[\mathrm{H}-3 \rightarrow \mathrm{L}]$ $-0.20\,[\mathrm{H}-1 \rightarrow \mathrm{L}+4]$
V	5.32	$-0.57\,[\mathrm{H} \rightarrow \mathrm{L}+4] - 0.50\,[\mathrm{H}-1 \rightarrow \mathrm{L}+3] + 0.34\,[\mathrm{H}-2 \rightarrow \mathrm{L}+2] + 0.30\,[\mathrm{H} \rightarrow \mathrm{L}+6]$ $-0.23\,[\mathrm{H}-3 \rightarrow \mathrm{L}+1]$
VI	5.71	$0.42\,[\mathrm{H}-4 \rightarrow \mathrm{L}+1] + 0.37\,[\mathrm{H}-5 \rightarrow \mathrm{L}] + 0.33\,[\mathrm{H}-1 \rightarrow \mathrm{L}+4] + 0.31\,[\mathrm{H}-3 \rightarrow \mathrm{L}+2]$ $+0.29\,[\mathrm{H}-1 \rightarrow \mathrm{L}+2]$

In this context it has to be taken into consideration that inelastic electron scattering experiments probe changes of electron momentum rather than absolute values. Therefore the observed spectra of poly(acetylene) and related compounds (here beta-carotene) are equivalent to the spectra of thienyl and phenyl based systems, in spite of the fact that in poly(acetylene) the lowest energy separation between the conduction and valence bands (i.e. the HOMO and LUMO positions in the quasi-band structure) is found at the boundary of the first Brillouin zone and not at its centre (see figure 2).

3.4. Molecular orbitals

It has been shown in [7] for a model molecule consisting of a linear chain of 18 benzene rings that the molecular states of quasi-periodic systems of that size possess a Bloch-like character. In beta-carotene there are also nine double bonds (plus the corresponding single bonds) in a row. The molecular states in figure 10 are already reminiscent of lattice periodically modulated plane waves as it is according to Bloch's theorem found in any fully periodic material. Consequently in beta-carotene the increasing number of nodes of the envelope functions for lower lying occupied and higher lying unoccupied states is well resolved. A similar orbital structure also prevails in 6P (see figure 11) and 6T [24].

A comparison of the beta-carotene orbitals in figure 10 with the molecular states in 6P in figure 11 reveals that the symmetry properties of the molecular orbitals involved in the description of the lower lying excited states are directly related to the momentum range associated with the HOMO and LUMO states in the quasi-band picture. In 6P the orbitals on each of the individual benzene rings do have the same symmetry (apart from the modulation by the plane wave part of the wavefunction). This means that the sign of the wavefunction (as represented by the shading) does not change between equivalent C atoms on different rings, unless the overall wavefunction has a node between those rings. In contrast to that the signs of the beta-carotene orbitals (i.e. shadings in figure 10) change for each of the subsequent double bonds. This can be viewed as a direct consequence of the fact that the HOMO and LUMO wavefunctions of beta-carotene are described by $\boldsymbol{k}$ values close to the boundary of the first Brillouin zone (see figure 2), which for the orbitals induces a phase shift of 180° between each of the repeat units. This according to figure 2 does not apply for 6P and 6T, which is verified by the orbital shapes in figure 11 and the data contained in [24].

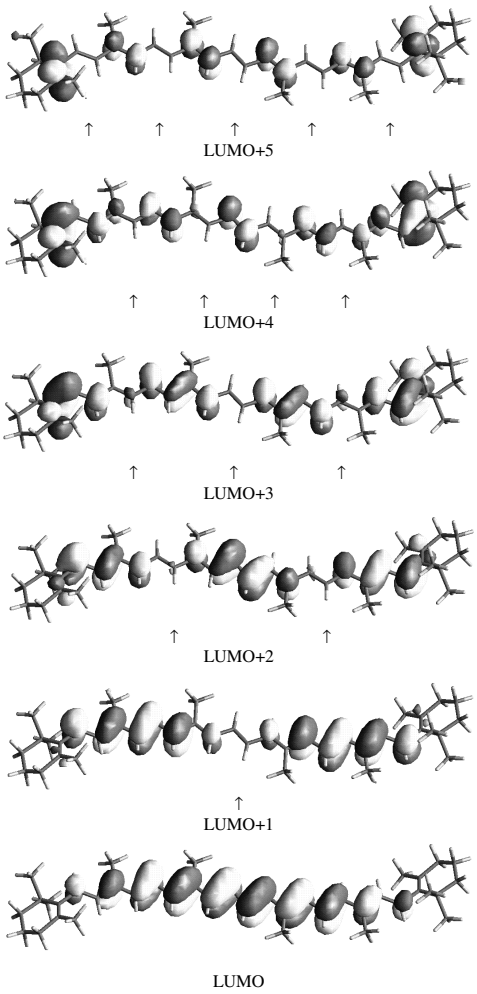

Figure 10. INDO calculated lowest unoccupied molecular orbitals of beta-carotene. For the occupied states a similar structure is obtained. (The dark and light shadings represent different signs of the wavefunctions and the arrows denote nodes of the plane-wave-like envelope function.)

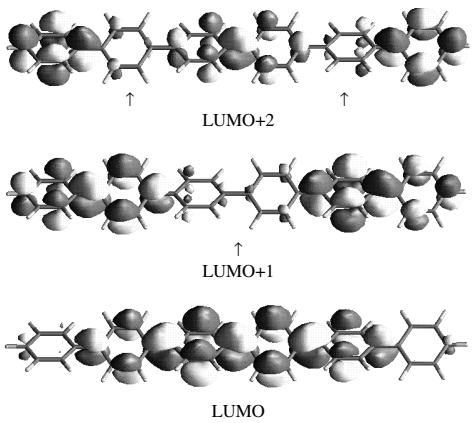

Figure 11. INDO calculated lowest unoccupied molecular orbitals of 6P. For the occupied states a similar structure is obtained. (The dark and light shadings represent different signs of the wavefunctions and the arrows denote nodes of the plane-wave-like envelope function.)

4. Conclusions

By combining semiempirical post-Hartree–Fock simulations of inelastic scattering cross-sections with experimental EELS studies for highly textured samples we have been able to show that the electronic structure of sexiphenyl, sexithienyl and beta-carotene in momentum space can be well described in the framework of the quasi-band structure. These particular materials have been selected for our studies as they are well defined model substances consisting of the most fundamental building blocks encountered in conjugated organic materials, namely phenylene and thienylene rings, as well as vinylene units. The full applicability of the quasi-band description to these model materials implies that a quasi-band

behaviour is a common feature at least in all organic materials possessing a certain degree of periodicity.

In the current paper we also discuss the possible effects that can lead to deviations between molecule-based simulations and inelastic electron scattering investigations and show that the angle between the molecular axis and the direction of momentum transfer crucially determines the experimentally observed dispersion. Consequently, care has to be taken when deriving the band width and dispersion from experimental EELS spectra of not perfectly oriented samples. Furthermore we note that the strong coupling between different single particle transitions in the CI description of the excited states shows that correlation effects do play a significant role in the description of excited states, resulting in certain deviations from a simple single particle picture.

Acknowledgments

We are strongly indebted to R Zamboni and C Taliani for providing the 6T thin films and to G Jakopic for fruitful discussions. The work in Graz has been financially supported by a *Doktorandenstipendium* of the Austrian Academy of Science and by the *Spezialforschungsbereich Elektroaktive Stoffe* of the Austrian *Fonds zur Förderung der wissenschaftlichen Forschung*. The work in Mons is partly supported by the Belgian Prime Minister Services for Scientific, Technical, and Cultural Affairs (*Pôle d'Attraction Interuniversitaire en Chimie Supramoléculaire et Catalyse*—PAI 4/11), FNRS/FRFC and an IBM–Belgium Academic Joint Study.

References

[1] Tang C W and VanSlyke S A 1987 *Appl. Phys. Lett.* **51** 913
Burroughes J H, Bradley D D C, Brown A R, Marks R N, Mackay K, Friend R H, Burn P L, Kraft A and Holmes A B 1990 *Nature* **347** 539
Pei Q, Yu G, Zhang Ch, Yang Y and Heeger A J 1995 *Science* **269** 1086
[2] Sariciftci N S, Smilowitz L, Heeger A J and Wudl F 1992 *Science* **258** 1474
Halls J J M, Walsh C A, Greenham N C, Marseglia E A, Friend R H, Moratti S C and Holmes A B 1995 *Nature* **376** 498
[3] Garnier F, Hajlaoui R, Yassar A and Srivastava P 1994 *Science* **265** 1684
Dodabalapur A, Torsi L and Katz H E 1995 *Science* **268** 270
[4] Grem G, Leditzky G, Ullrich B and Leising G 1992 *Adv. Mater.* **4** 36
Era M, Tsutsui T and Saito S 1996 *Appl. Phys. Lett.* **67** 2436
[5] See e.g. Menon R, Yoon C O, Moses D and Heeger A J 1998 *Handbook of Conducting Polymers* ed T A Skotheim, R L Elsenbaumer and J R Reynolds (New York: Dekker)
[6] Bredas J L, Silbey R, Boudreaux D S and Chance R R 1983 *J. Am. Chem. Soc.* **105** 6555
[7] Zojer E, Shuai Z, Leising G and Brédas J L 1999 *J. Chem. Phys.* **111** 1668
[8] Fink J 1989 *Adv. Electron. Electron Phys.* **75** 121 and references therein
[9] Pellegrin E, Fink J and Drechsler S L 1991 *Phys. Rev. Lett.* **66** 2022
Pellegrin E, Fritzsche H, Nücker N, Fink J, Drechsler S L, Málek J, Meerholz K, Heinze J and Roth S 1991 *Synth. Met.* **41–43** 1207
[10] Zojer E, Knupfer M, Resel R, Meghdadi F, Leising G and Fink J 1997 *Phys. Rev.* B **56** 10 138
[11] Knupfer M, Pichler T, Golden M S, Fink J, Murgia M, Michel R H, Zamboni R and Taliani C 1999 *Phys. Rev. Lett.* **83** 1443
[12] Salem L 1966 *The Molecular Orbital Theory of Conjugated Systems* (New York: Benjamin)
[13] Hoffmann R 1988 *Solids and Surfaces: a Chemist's View of Bonding in Extended Structures* (New York: VCH)
[14] Narioka S, Ishii H, Edamatsu K, Kamiya K, Hasegawa S, Ohta T, Ueno N and Seki K 1995 *Phys. Rev.* B **52** 2362
[15] Pople J A, Beveridge D L and Dobosh P A 1967 *J. Chem. Phys.* **47** 2026
[16] Shuai Z, Zojer E, Leising G and Brédas J L 1999 *Synth. Met.* **101** 337

[17] Dewar M J S, Zoebisch E G, Healy E F and Stewart J J P 1985 *J. Am. Chem. Soc.* **107** 3902
[18] Compare Baudour J L, Cailleau H and Yelon W B 1977 *Acta Crystallogr.* B **33** 1773
Baudour J L, Delugeard Y and Rivet P 1978 *Acta Crystallogr.* B **34** 625
[19] Zojer E, Cornil J, Leising G and Brédas J L 1999 *Phys. Rev.* B **59** 7957
[20] Baker K N, Fratini A V, Resch T, Knachel H C, Adams W W, Socci E P and Farmer B L 1993 *Polymer* **34** 1571
[21] Puschnig P and Ambrosch-Draxl C 1999 *Phys. Rev.* B **60** 7891
[22] Horowitz G, Bachet B, Yassar A, Lang P, Demanze F, Fave J-L and Garnier F 1995 *Chem. Mater.* **7** 1337
[23] Sterling C 1964 *Acta Crystallogr.* **17** 1224
[24] Zojer E 1999 *PhD Thesis* Technische Universität Graz
[25] Zerner M C, Loew G H, Kichner R F and Mueller-Westerhoff U T 1980 *J. Am. Chem. Soc.* **102** 589
[26] Mataga N and Nishimoto K 1957 *Z. Phys. Chem.* **13** 140
[27] Compare e.g. Jones W and March N H 1973 *Theoretical Solid State Physics* vol 1 (London: Wiley–Interscience) (1973; republished by Dover Publications, Mineola) p 451 ff
[28] Era M, Tsutsui T and Saito S 1996 *Appl. Phys. Lett.* **67** 2436
[29] Rice M J and Gartstein Yu N 1994 *Phys. Rev. Lett.* **73** 2504
Comoretto D, Dellepiane G, Moses D, Cornil J, dos Santos D A and Bredas J L 1998 *Chem. Phys. Lett.* **289** 1
Miller E K, Yoshida D, Yang C Y and Heeger A J 1999 *Phys. Rev.* B **59** 4661
[30] Cornil J, Heeger A J and Bredas J L 1997 *Chem. Phys. Lett.* **272** 463
Cornil J, dos Santos D A, Crispin X, Silbey R and Brédas J L 1998 *J. Am. Chem. Soc.* **120** 1289
Muccini M, Lunedei E, Taliani C, Beljonne D, Cornil J and Brédas J L 1998 *J. Chem. Phys.* **109** 10 513
[31] da Costa P, Dandrea R G and Conwell E M 1993 *Phys. Rev.* B **47** 1800
[32] Ambrosch-Draxl C, Majewski J A, Vogl P and Leising G 1995 *Phys. Rev.* B **51** 9668
Ambrosch-Draxl C, Majewski J A, Vogl P, Leising G, Abt R and Aichholzer K D 1995 *Synth. Met.* **69** 411